The Astrophysical Journal, 835:80 (9pp), 2017 January 20 doi:10.3847/1538-4357/835/1/80

STELLAR, GAS, AND DARK MATTER CONTENT OF BARRED GALAXIES

Bernardo Cervantes Sodi
Instituto de Radioastronomía y Astrofísica, Universidad Nacional Autónoma de México, Campus Morelia, A.P. 3-72, C.P. 58089 Michoacán, México;
b.cervantes@crya.unam.mx
Received 2016 July 6; revised 2016 November 14; accepted 2016 November 18; published 2017 January 19

ABSTRACT

We select a sample of galaxies from the Sloan Digital Sky Survey Data Release 7 (SDSS-DR7) where galaxies are classified, through visual inspection, as hosting strong bars, weak bars, or as unbarred galaxies, and make use of H I mass and kinematic information from the Arecibo Legacy Fast ALFA survey catalog, to study the stellar, atomic gas, and dark matter content of barred disk galaxies. We find, in agreement with previous studies, that the bar fraction increases with increasing stellar mass. A similar trend is found with total baryonic mass, although the dependence is not as strong as with stellar mass, due to the contribution of gas. The bar fraction shows a decrease with increasing gas mass fraction. This anticorrelation between the likelihood of a galaxy hosting a bar with the gas richness of the galaxy results from the inhibiting effect the gas has in the formation of bars. We also find that for massive galaxies with stellar masses larger than 10^{10} $M_{\odot}$, at fixed stellar mass, the bar fraction decreases with increasing global halo mass (i.e., halo mass measured up to a radius of the order of the H I disk extent).

Key words: galaxies: fundamental parameters – galaxies: halos – galaxies: spiral – galaxies: statistics – galaxies: structure

1. INTRODUCTION

In the local universe, a substantial percentage of massive galaxies are known to present stellar bars (e.g., de Vaucouleurs et al. 1991; Eskridge et al. 2000; Laurikainen et al. 2004; Buta et al. 2010, 2015; Nair & Abraham 2010; Cervantes Sodi et al. 2015, henceforth CS+15; Gavazzi et al. 2015).

Given the non-axisymmetric nature of bars, they are expected to speedup secular evolution in galaxies, leading to mass and angular momentum redistribution within the components of the galaxies (Lynden-Bell 1979; Roberts et al. 1979; Sellwood 1981; Weinberg 1985; Sellwood & Wilkinson 1993; Athanassoula 2003; Kormendy & Kennicutt 2004; Cheung et al. 2013; Sellwood 2014).

The origin of stellar bars has been addressed from the first numerical simulations, starting with the pioneering work by Ostriker & Peebles (1973) where they simulated galaxies with hundreds of mass points, and found that all of their simulated systems were unstable to barlike modes, but the inclusion of a spherical halo component with a halo-to-disk mass ratio larger than 1, was enough to prevent the formation of bars. They proposed a stability criterion based on the ratio of the kinetic energy of rotation over total gravitational energy, with a marginal value of 0.14 for reaching stability. In a similar way, Efstathiou et al. (1982), through numerical experiments, proposed their own stability criterion in terms of the maximum rotation curve velocity ($v_{\rm max}$), and the mass and scale-length of the disk ($M_{\rm d}$, $f_{\rm d}$), defined as $\epsilon_c = v_{\rm max}/({\rm G}M_{\rm d}/r_{\rm d})^{1/2} > 1.1$ for stable systems. In this sense, ϵ_c gives a measure of the self-gravity of the disk (see also Christodoulou et al. 1995). Athanassoula & Sellwood (1986), using two-dimensional (2D) simulations, confirmed the analytical result by Toomre (1981), that a higher halo-to-disk mass ratio decreases the bar growth rate, but also pointed out the relevance of random motions within the disk, that also help to stabilize the disk against bar formation, even for maximal disks.

The effects of the halo on bar formation and growth are not as simple as they seemed in early works. For instance, the strength of the bar and the decrease of its pattern speed are set by the amount of angular momentum that is able to be lost. A responsive dark matter halo can work as a sink of angular momentum, allowing the growth of bars in the secular evolution phase, although in the formation phase the presence of a massive halo slows down their formation (Athanassoula 2002, 2003, 2013 for a review). Debattista & Sellwood (2000) concluded that in order to maintain their observed high pattern speeds, bars must be hosted by low central density halos, because for dense halos the drag force due to dynamical friction between the bar and the halo is enough to drive the corotation point out to unrealistic distances; in this way, not only the mass of the halo is relevant, but also its density. The triaxiality of halos produces significant effects on the origin and fate of bars. Triaxial halos induce early bar formation (Berentzen et al. 2006; Athanassoula et al. 2013), but once the bar is formed, they damp their growth (Berentzen et al. 2006; Machado & Athanassoula 2010; Athanassoula et al. 2013). If a rotating halo is included, the growth in size and strength of bars gets quenched with increasing spin (Saha & Naab 2013; Long et al. 2014), which explains why the bar fraction decreases with increasing spin (Cervantes-Sodi et al. 2013).

Although the interaction between the halo component and the bar is complex, results from recent simulations converge on the idea that the disk-to-halo mass ratio is a factor of primary importance in bar formation and evolution. In some cases, bar formation is suppressed if the halo mass is increased (DeBuhr et al. 2012; Yurin & Springel 2015), while in some other cases, the bars are produced even in simulated galaxies with low disk-to-halo mass ratios, but the amplitude of the bars is smaller in halo dominated systems, and the growth of the bar slows down (Sellwood 2016).

The effects of the disk-to-halo mass ratio on bar formation and evolution have also been studied from an observational perspective. Working with a sample of bright barred and unbarred galaxies, Courteau et al. (2003) found that for a given luminosity, the structural and dynamical parameters of the two subsamples are comparable, with barred and unbarred galaxies following the same Tully–Fisher relation, which implies that at

fixed luminosity, barred and unbarred galaxies have halos of comparable mass. More recently, using a volume-limited sample of galaxies from the Slona Digital Sky Survey (SDSS), with halo masses taken from the Yang et al. (2007) galaxy group catalog, CS+15 found a strong correlation between the fraction of galaxies hosting strong bars and the stellar-to-halo mass ratio, with f_{bar} increasing with increasing M_*/M_{halo}, even at fixed stellar mass. Díaz-García et al. (2016) found a similar dependence of the bar fraction with M_*/M_{halo}, but the dependence in their sample vanishes at fixed stellar mass. This question will be addressed in the present work.

Observational studies have shown that bars are more frequently found in massive, red galaxies with early-type morphologies and prominent bulges (Erwin 2005; Sheth et al. 2008; Weinzirl et al. 2009; Nair & Abraham 2010; Hoyle et al. 2011; Lee et al. 2012a, henceforth Lee+12; Cervantes-Sodi et al. 2013), highlighting that the formation of bars is strongly dependent on the physical properties of the hosting galaxy. Results by Sheth et al. (2008) and Kraljic et al. (2012) show a dramatic decline of the bar fraction with increasing redshift for low-mass galaxies, while the bar fraction in massive, luminous galaxies remains constant out to $z \sim 0.8$. This suggests that bars form later in low mass galaxies, in a downsizing way, with bars forming at the same epoch at which galaxies become kinematically cold, dominated by a thin stellar disk. One crucial component in the formation process and evolution of bars is the fraction of mass in the form of gas in the galaxy. When a galaxy is rich in gas, a significant exchange of angular momentum is expected to occur between the stellar and gas components (Friedli & Benz 1993; Athanassoula 2003; Combes 2008). In this exchange, the angular momentum lost by the gas is transferred to the bar, letting the gas inside the co-rotation radius fall to the central region and preventing the inflow of gas from external regions (Athanassoula 1992; Heller & Shlosman 1994; Knapen et al. 1995; Sheth et al. 2005). At the same time, the interchange of angular momentum increases the rotation frequency of the bar, weakening it and ultimately destroying it (Combes 2008). Recent simulations including feedback, cooling, and star formation (Athanassoula et al. 2013) have also shown that bars in the presence of large amounts of gas are expected to form later, and at all times are weaker, than in gas-poor simulations.

The effect of gas on the structure of the bar can be due to an indirect process, as suggested by Berentzen et al. (2007), with the bar fuelling gas to the center of the galaxy, where it grows a central mass concentration (CMC) that weakens the bar. This inflow of gas to the center can in turn produce a central starburst as predicted by simulations (Shlosman et al. 1989, Berentzen et al. 1998) and confirmed by some observational studies (Laurikainen et al. 2004; Jogee et al. 2005; Ellison et al. 2011; Wang et al. 2012). In the end, the result of enhanced central star formation in barred galaxies, and the adverse effects of gas on the evolution of the bar, could explain why the bar fraction observed in local galaxies decreases for increasing gas mass fraction (Masters et al. 2012; Cheung et al. 2013).

In this paper we study the dependence of the bar fraction on the stellar-to-halo mass ratio following CS+15 but using a more direct approach to estimate halo masses. Instead of using a method that depends on the clustering of galaxies and assumes a one-to-one relation between the total luminosity of the groups and the halo mass, here we explore a more direct approach, assigning halo masses using kinematic information from H I line widths. We also study the dependence of the bar fraction on the gas mass ratio with the aim to disentangle if the decrease of the bar fraction on gas-rich galaxies is caused by bars promoting the consumption of gas and/or if the increase of gas content inhibits bar formation. The main results and discussion are presented in Section 3. Lastly, we summarize our general conclusions in Section 4. Throughout this paper, we use a cosmology with density parameter $\Omega_m = 0.3$, cosmological constant $\Omega_\Lambda = 0.7$ and Hubble constant written as $H_0 = 100h\,\mathrm{km\,s^{-1}\,Mpc^{-1}}$, with $h = 0.7$.

2. DATA

2.1. Galaxy Catalog

The parent galaxy sample used in this work consist of nearly ~30,000 galaxies (Lee+12) drawn from the SDSS Data Release 7 (DR7; Abazajian et al. 2009). It is selected as a volume-limited sample, within the redshift range $0.02 \leqslant z \leqslant 0.05489$, and complete down to a limit r-band absolute magnitude brighter than $M_r = -19.5 + 5\log h$. The morphological classification of the sample is obtained using the method developed by Park & Choi (2005), where galaxies are segregated into early- and late-types in the color versus color gradient and concentration index planes. For the present study we keep only late-type galaxies.

The bar identification is obtained by visual inspection of combined color images of three SDSS bands ($g + r + i$), and once a bar is identified is further classified as a strong bar if its length is larger than one quarter of the optical size of the host galaxy, or as a weak bar otherwise. We further restrict the sample to those galaxies with i-band isophotal axis ratio $b/a > 0.6$, a and b being the semimajor and semi-minor axes, in order to avoid selection biases by inclination, given that bars are easier to identify in face-on galaxies. Keeping only late-type galaxies mostly face-on reduces the parent sample to 10,674 galaxies, of which 23.8% host strong bars and 6.5% host weak bars, giving a total bar fraction of 30.4%. A detailed comparison of this volume limited sample is presented in Section 3.2 of Lee+12, where the authors show a good agreement with the classification performed by Nair & Abraham (2010). Furthermore, the dependence of the bar fraction of the sample on stellar mass, color, and concentration index are in qualitative and quantitative good agreement with the findings by Nair & Abraham (2010), Masters et al. (2011), and Oh et al. (2012). We refer the reader to Lee+12 for a more detailed description of the sample, along with a number of studies that make use of this same sample (Lee et al. 2012b; Cervantes-Sodi et al. 2013; Lin et al. 2014; Cervantes Sodi et al. 2015).

The optical photometric properties required for this study are extracted from the Korea Institute for Advanced Study Value-Added Galaxy Catalog (Choi et al. 2010), together with the NASA Sloan Atlas3 (NSA) catalog (Blanton et al. 2011), from where we get the stellar masses of our galaxies. The stellar masses in the NSA are calculated using SDSS and *GALEX* photometric bands and the *kcorrect* software by Blanton & Roweis (2007), assuming a Chabrier (2003) initial mass function. The estimations of star formation rates (SFRs) and specific star formation rates (sSFRs) come from the New York University Value Added Galatic Catalog (NYU-VAGC;

Blanton et al. 2005) and the MPA/JHU SDSS database (Kauffmann et al. 2003; Brinchmann et al. 2004).

2.2. H I Data

To estimate dynamical masses and halo masses for the galaxies in our sample, as well as gas mass fractions, we turn to the ALFALFA survey (Giovanelli et al. 2005), which is a blind, single-dish, flux-limited extragalactic H I survey. We use data from the publicly available catalog of the ALFALFA survey "α.70," which covers about 70% of the final survey area, which is planed to be 7000 deg^2 of high galactic latitude sky observable with the telescope and an expected detection of >30,000 galaxies, out to $cz \approx 18{,}000$ km s^{-1}. A description of the "α.40" catalog can be found in Haynes et al. (2011).

H I masses are estimated using the formula by Haynes & Giovanelli (1984);

$$M_{\rm H\,I} = 2.356 \times 10^5 \left(\frac{D}{\rm Mpc}\right)^2 \frac{S_{21}}{\rm Jy\ km\ s^{-1}} [M_\odot] \quad (1)$$

where S_{21} is the integrated H I line flux density in units of Jy km s^{-1}, and D is the distance in Mpc. From the H I mass, we estimate the atomic gas mass as $M_{\rm gas} = 1.4\ M_{\rm H\,I}$, where the numeric factor 1.4 is introduced to account for the presence of helium. The baryonic mass is simply $M_{\rm baryon} = M_{\rm gas} + M_*$.

To calculate dynamical masses for the galaxies in the sample, we first estimate the galactic rotational velocity as

$$V_{\rm rot} = W/(2 \times \sin i), \quad (2)$$

where W is the H I line width measured at 50% of the peak flux, in units of km s^{-1}, as provided by the ALFALFA α.70 catalog, and i is the inclination angle of the galaxy, which is computed through the expression

$$\cos^2 i = \frac{(b/a)^2 - q_0^2}{1 - q_0^2}, \quad (3)$$

with $q_0 = 0.13$ assumed for the intrinsic axial ratio of galaxies viewed edge-on (Giovanelli et al. 1994). The output of the match of our parent sample with the α.70 catalog gives a total of 1471 galaxies for our study, which is primarily limited by the ALFALFA detection limits, imposing a bias toward gas-rich systems. From the total sample, 293 (20%) are galaxies hosting strong bars, 106 (7%) host weak bars, and 1072 (73%) are unbarred galaxies. The low fraction of barred galaxies in the sample is due to the strict classification criteria used to identify bars and the bias toward gas-rich galaxies, that as we show in Section 3.3, present a lower bar fraction when compared with gas-poor systems.

3. RESULTS AND DISCUSSION

3.1. Bar Fraction as a Function of Mass

We start our analysis by looking at the dependence of the bar fraction $f_{\rm bar}$ as a function of different masses defined for our sample. In Figure 1(a), we show the dependence of the bar fraction on stellar mass for strong and weak bars, as well as for strong plus weak bars, with the well known trend of higher $f_{\rm bar}$ for galaxies with high stellar masses (Masters et al. 2012; Oh et al. 2012; Skibba et al. 2012; Cervantes-Sodi et al. 2013; Gavazzi et al. 2015) at least for the case of strong bars; an expected result given that bars form earlier in massive galaxies, as previously shown by Sheth et al. (2008) and Kraljic et al. (2012). Error bars in all figures denote estimated 1σ confidence intervals based on the bootstrapping resampling method. The corresponding result using baryonic mass is presented in Figure 1(b), where a slight increase of the bar fraction for increasing baryonic mass is noticeable, but the trend is less dramatic than the one present as a function of stellar mass. This might be due to the fact that an increase in $M_{\rm baryon}$ can be the result of an increase of M_* but also an increase of $M_{\rm gas}$. And as will be discussed in Section 3.3, an increase of M_* promotes the growth of the bar, but an increase of $M_{\rm gas}$ hinders the growth of the bar.

To study the dependence of the bar fraction on halo mass, following Bradford et al. (2015), we employ two different estimates. We calculate the dynamical mass $M_{\rm dyn}$, as the mass responsible for establishing a flat rotation curve with amplitude $V_{\rm rot}$ within the H I disk radius;

$$M_{\rm dyn} = \frac{R_{\rm H\,I} V_{\rm rot}^2}{G}. \quad (4)$$

Given that we do not count with rotation curves, we follow Broeils & Rhee (1997) to estimate the radius of the H I disk ($R_{\rm H\,I}$) in terms of the H I mass using one of the tightest scaling relations of galaxy disks (Lelli et al. 2016):

$$\log M_{\rm H\,I} = 1.96\ log\ D_{\rm H\,I} + 6.52, \quad (5)$$

with $R_{\rm H\,I} = D_{\rm H\,I}/2$. By using Equation (4), we are measuring the halo mass to a distance from the center that extends to the radius of the H I disk, which typically extends to twice the optical size of the galaxies (Broeils & Rhee 1997). The fraction of barred galaxies as a function of dynamical mass is shown in Figure 1(c), where $f_{\rm bar}$ seems to be independent of $M_{\rm dyn}$.

As a second estimate for the halo mass we turn to the study by van den Bosch (2002), where he explored different virial mass estimators for disk galaxies using models for the formation of these kind of galaxies. The best estimator, with the smallest scatter, is a combination of circular velocity and disk scale radius $r_{\rm d}$, of the form

$$M_{\rm halo} = 2.54 \times 10^{10} M_\odot \left(\frac{r_{\rm d}}{\rm kpc}\right)\left(\frac{V_{\rm rot}}{100\ \rm km\ s^{-1}}\right)^2. \quad (6)$$

The result using $M_{\rm halo}$ (Figure 1(d)) is very similar to the one using $M_{\rm dyn}$, with little or no dependence of the bar fraction on either of these mass estimates, a result in agreement with Martínez & Muriel (2011) and Wilman & Erwin (2012) who found no evidence of bars preferring any particular halo mass.

3.2. Bar Fraction as a Function of Stellar and Baryonic Fractions

In CS+15, the authors showed that a strong dependence is found for the bar fraction with the stellar-to-halo mass fraction, with the dependence present for strong bars in massive systems even at fixed stellar mass. In this section we explore if our sample presents this same dependence. Figures 2(a) and (c) present the bar fraction as a function of the stellar-to-dynamic mass and the stellar-to-halo mass ratio, respectively, showing the same behavior as the one reported by CS+15 using a totally independent method, with the fraction of strong bars increasing systematically with increasing mass ratio.

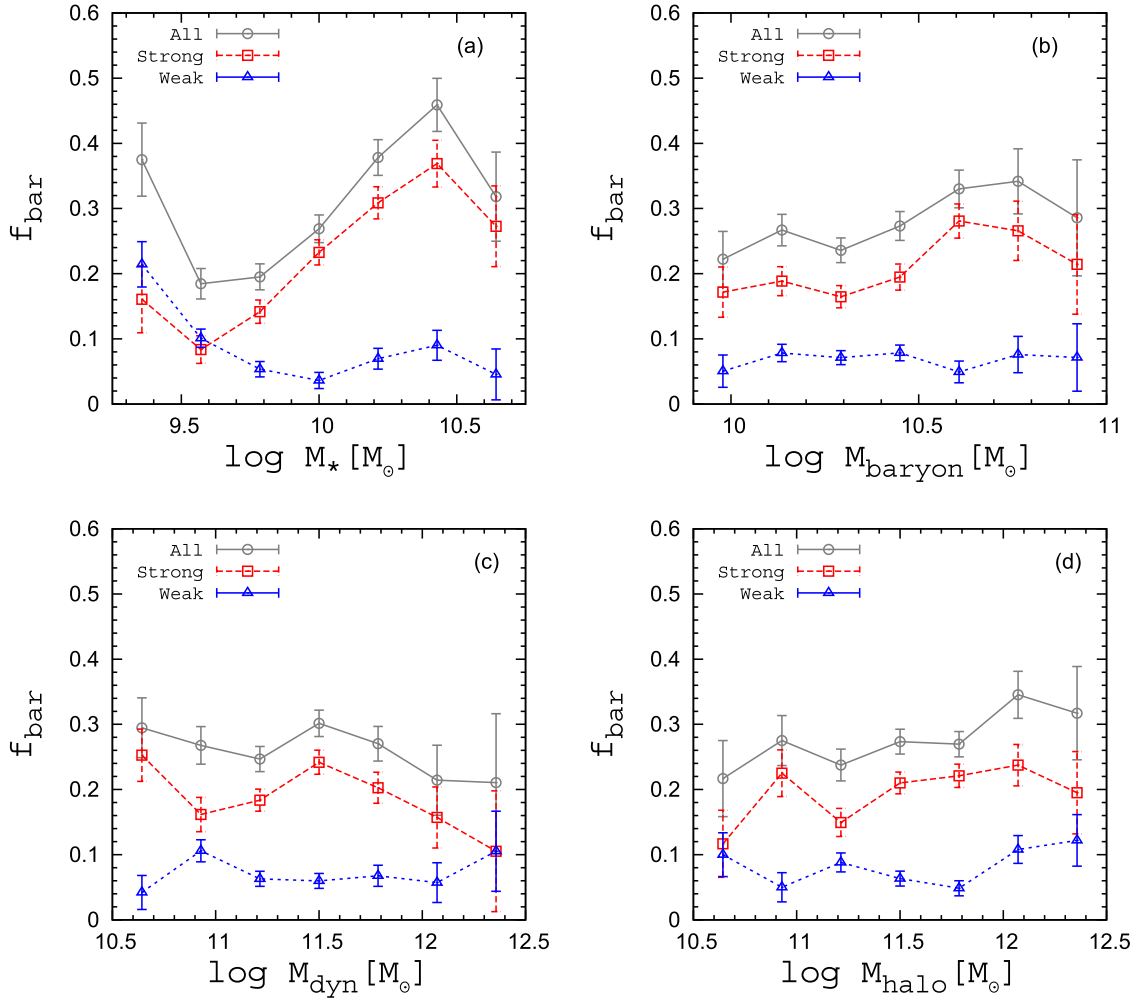

Figure 1. Fraction of barred galaxies $f_{\rm bar}$ as a function of (a) stellar mass M_*, (b) baryonic mass $M_{\rm baryon}$, (c) dynamic mass $M_{\rm dyn}$, and (d) halo mass $M_{\rm halo}$.

Having estimated the baryonic mass for the galaxies of the sample, we also present the bar fraction as a function of baryonic-to-dynamic mass and baryonic-to-halo mass ratios in Figures 2(b) and (d). Figure 2(b) shows a weak dependence of the bar fraction for strong bars on the baryonic-to-dynamic mass ratio, much weaker than the one presented in Figure 2(a) with the stellar-to-dynamic mass ratio. Finally, Figure 2(d) shows no dependence of the bar fraction on the baryonic-to-halo mass ratio. The difference in the behavior of $f_{\rm bar}$ with the mass ratios using stellar mass and baryonic mass comes from the inclusion of the gas component, which we will explore in more detail in Section 3.3.

The increase of $f_{\rm bar}$ with increasing $M_*/M_{\rm halo}$ and $M_*/M_{\rm dyn}$, given the little dependence of the bar fraction on $M_{\rm dyn}$ and $M_{\rm halo}$, must be preferentially driven by the dependence on M_*. In what follows, we will explore the dependence of the bar fraction on the halo mass at fixed stellar mass.

In Figure 2(a) of CS+15, the authors show that the bar fraction in the $M_{\rm halo}$ versus M_* plane presents a dependence on the halo mass even at fixed stellar mass, especially for the case of strong bars where the effect is clear, with $f_{\rm bar}$ increasing for decreasing $M_{\rm halo}$ at fixed M_*. For the case of weak bars, the dependence is weak and goes in the opposite direction.

Díaz-García et al. (2016) also explored the dependence of the bar fraction on the stellar-to-halo mass ratio using a smaller sample than the one used by CS+15, but their estimate of $M_*/M_{\rm halo}$ is a more direct one that the one used by CS+15, comparing the circular velocity curve inferred from infrared images with inclination-corrected H I velocity amplitude as obtained from various sources (Courtois et al. 2009, 2011 and HyperLEDA). When using Fourier and ellipse fitting methods to detect bars, Díaz-García et al. (2016) obtained the same tendency of $f_{\rm bar}$ decreasing with increasing $M_{\rm halo}/M_*$ ratio, but they reported that this tendency is suppressed at fixed stellar mass.

To test if in our sample the dependence of $f_{\rm bar}$ on $M_*/M_{\rm halo}$ and $M_*/M_{\rm dyn}$ vanishes at fixed stellar mass, we follow CS+15 exploring the behavior of the strong bar fraction in the $M_{\rm halo}$ versus M_* and $M_{\rm dyn}$ versus M_* planes. To get a smooth transition of $f_{\rm bar}$, we use a spline kernel, dividing the plane in 10×10 regions where $f_{\rm bar}$ is estimated, requiring a minimum of 10 galaxies per region. This combination is chosen after testing different bin sizes and the minimum galaxies requested on each bin, by generating mock samples from the same parent sample and varying the combination of these two parameters until the contours cease to fluctuate from sample to sample. The contours in Figure 3 show that the maximum value of $f_{\rm bar}$ is reached in the region denoted by $M_* > 10^{10.25}\ M_\odot$ and $M_{\rm dyn}$, $M_{\rm halo} < 10^{11}\ M_\odot$. The contours in both panels of Figure 3 also show that there is an increase of $f_{\rm bar}$ with increasing M_*, and for massive galaxies with $M_* > 10^{10}\ M_\odot$, an increase of the bar fraction with decreasing $M_{\rm dyn}$ and $M_{\rm halo}$, showing that even

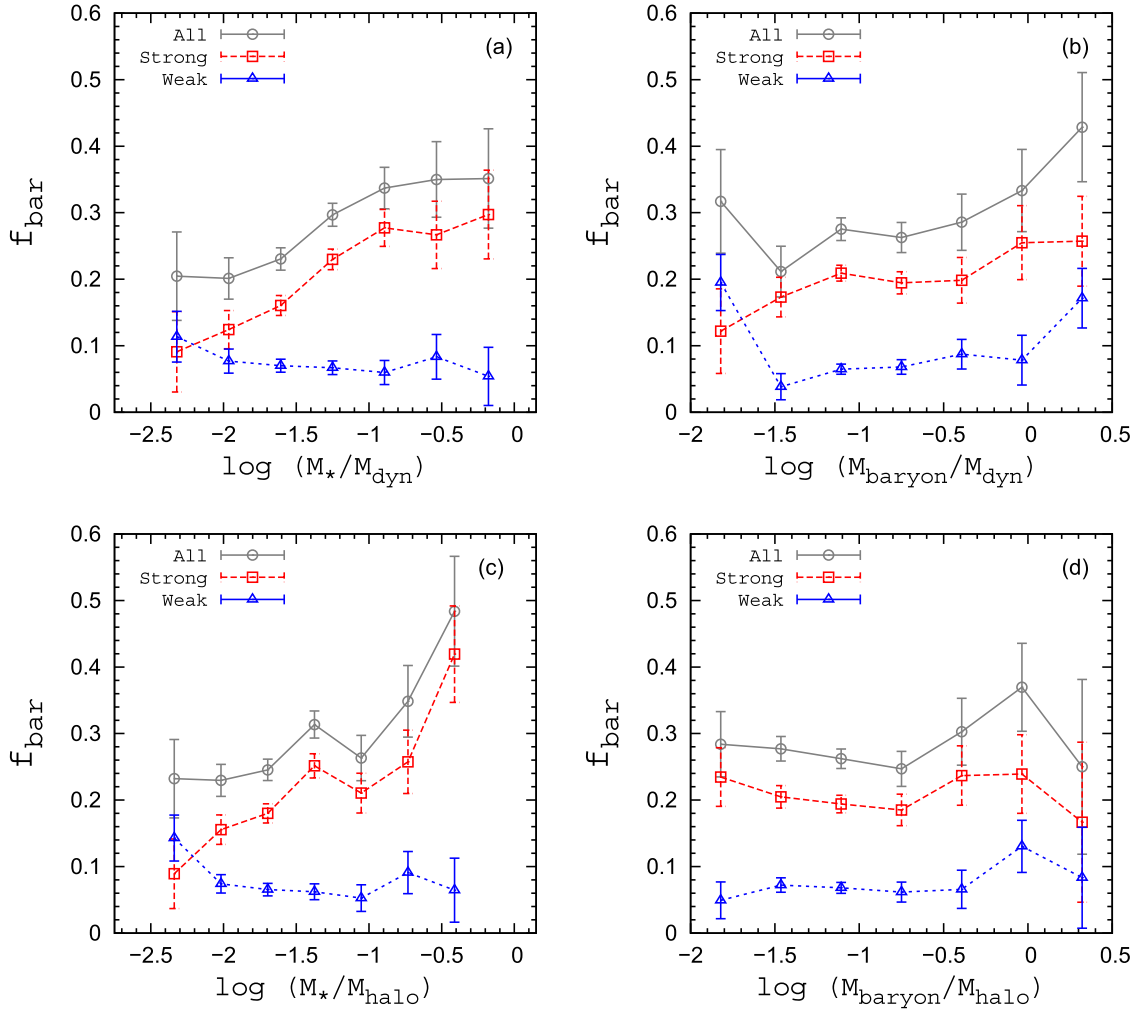

Figure 2. Fraction of barred galaxies $f_{\rm bar}$ as a function of (a) stellar-to-dynamic mass ratio $M_*/M_{\rm dyn}$, (b) baryonic-to-dynamic mass ratio $M_{\rm baryon}/M_{\rm dyn}$, (c) stellar-to-halo mass ratio $M_*/M_{\rm halo}$, and (d) bayonic-to-halo mass ratio $M_{\rm baryon}/M_{\rm halo}$.

at fixed stellar mass, there is a dependence of the bar fraction on $M_{\rm dyn}$ and $M_{\rm halo}$.

Another way to present this same result is to look at the bar fraction as a function of stellar mass, dividing the sample in two according to its dynamic mass and halo mass. In Figure 4 (left panels) is shown the bar fraction as a function of stellar mass for the full sample in the top panel, strong bars in the middle panel, and weak bars in the bottom panel. Each bin is further divided in half according to their dynamic mass, the solid (red) line corresponds to the subsample with high $M_{\rm halo}$ values while the broken (blue) line to the subsample with low $M_{\rm dyn}$ values. The top and middle panels show that massive galaxies ($M_* \geqslant 10^{10} M_\odot$) with low $M_{\rm halo}$ values have systematically higher bar fraction than galaxies with high $M_{\rm halo}$. For the case of weak bars, no systematic difference is found between the two subsamples.

The right panels of Figure 4 present the same analysis but using $M_{\rm dyn}$ instead of $M_{\rm halo}$, showing the same systematic variation but with greater significance, in good agreement with the results by CS+15. This result is also in line with recent simulations where it is found that the disk-to-halo mass ratio is a factor of primary importance in bar formation and evolution. In some of these studies (DeBuhr et al. 2012; Yurin & Springel 2015), bar formation is suppressed if the halo mass is increased, while in other cases bars are formed even in simulated galaxies with low disk-to-halo mass ratios, but the amplitude of the bars is smaller in halo dominated systems (Sellwood 2016).

We recall that we are dealing with global, integrated properties of galaxies, and that this strong dependence of the bar fraction with the stellar-to-halo mass and the stellar-to-dynamic mass ratio might change if we focus on the mass contribution of the halo in the central regions of the galaxy, given that it is only the mass in the relatively inner part of the halo that can interact with the bar (Athanassoula & Misiriotis 2002). In this regard, the results by Cervantes-Sodi et al. (2013) are complementary. They show that the bar fraction decreases for increasing spin, and if low surface brightness galaxies reside in halos with large values of spin (Jimenez et al. 1998; Kim & Lee 2013), these galaxies being dark matter dominated even in the central regions, then galaxies dominated by their dark matter component in the inner parts appear to be more stable against bar formation. The results shown in the present study, in combination with the results by CS+15 and Cervantes-Sodi et al. (2013), suggest that gravitational dominant stellar disks, both in the inner parts of the galaxy as well as globally, are more prone to develop and maintain stellar bars, in good agreement with what was reported by Algorry et al. (2016) studying the formation of 269 disks in a Lambda-cold dark matter (ΛCDM) cosmological

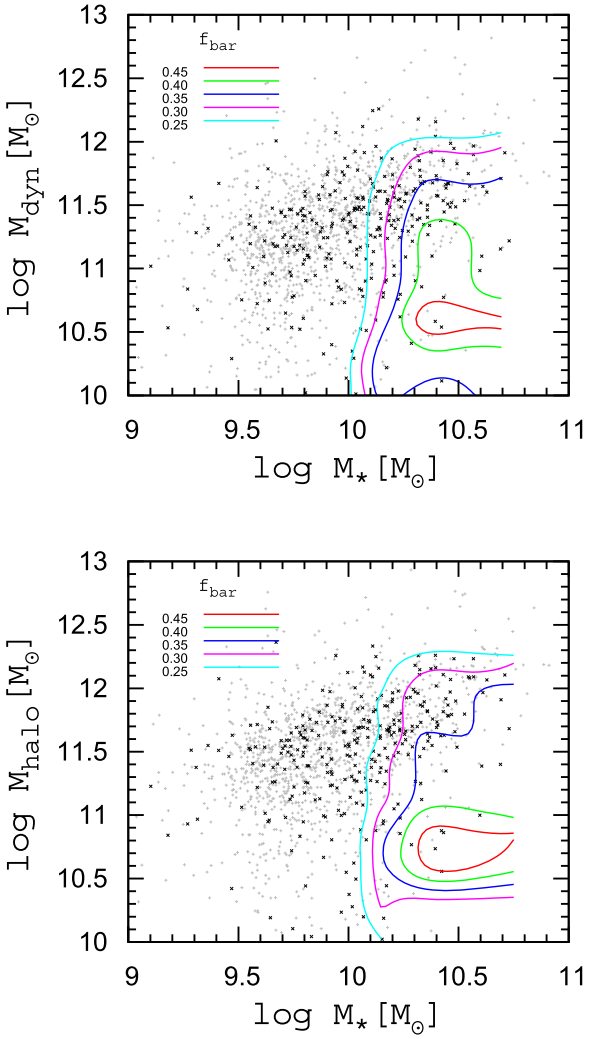

Figure 3. Bar fraction $f_{\rm bar}$ isocontours in the $M_{\rm dyn}$ vs. M_* (top panel) and $M_{\rm halo}$ vs. M_* (bottom panel) for strong bars. Contours denote regions of constant $f_{\rm bar}$ in the range $0.25 \leqslant f_{\rm bar} \leqslant 0.45$. Gray dots represent unbarred galaxies, black dots represent barred ones.

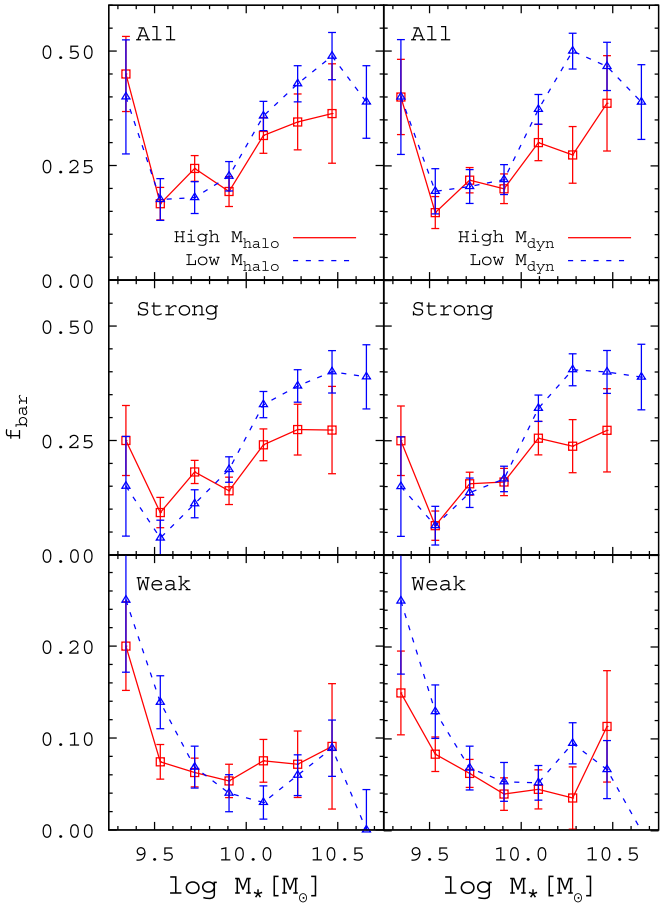

Figure 4. Fraction of barred galaxies $f_{\rm bar}$ as a function of M_* for the full sample (strong plus weak bars, top panels), strong bars (middle panels), and weak bars (bottom panels). For each bin a pair of values is plotted, in solid (red) lines galaxies with high $M_{\rm halo}$, values and in broken (blue) lines galaxies with low $M_{\rm halo}$ values. Right panels present the same as left panels but the sample is segregated using $M_{\rm dyn}$ instead of $M_{\rm halo}$.

hydrodynamical simulation from the EAGLE project, where 82% of their identified strong bars are hosted by simulated galaxies that satisfy a combined criteria of presenting a gravitational dominant disk within the half-mass–radius, and have a declining rotation curve beyond the outer confines of the disk.

3.3. Bar Fraction as a Function of H I Richness

In Figure 5 (top panel) we observe an anticorrelation between the bar fraction and the H I gas mass fraction, particularly clear for strong bars. The fraction of weak bars actually shows a positive correlation, with a mild increase of $f_{\rm bar}$ with increasing $M_{\rm H\,I}/M_*$. With the gas mass fraction decreasing for increasing stellar mass, the decrease of $f_{\rm bar}$ with increasing $M_{\rm H\,I}/M_*$ could be a direct consequence of the dependence of $f_{\rm bar}$ on the stellar mass. To test if $f_{\rm bar}$ depends directly on the H I gas mass fraction, we present the bar fraction for strong bars in the $M_{\rm H\,I}/M_*$ versus M_* plane in Figure 5 (bottom panel). The contours show a clear joint dependence of $f_{\rm bar}$ on both the stellar mass and the H I gas mass fraction, so even at fixed M_*, the strong bar fraction presents a clear dependence on $M_{\rm H\,I}/M_*$, as previously pointed out by Masters et al. (2012). We are not including molecular gas in the discussion because the typical molecular-to-atomic ratio is only ∼0.3, and given that the position of galaxies when plotted in the SFR versus M_* plane can be explained by their global cold gas reservoirs as determined through the H I line (Saintonge et al. 2016), we do not expect its inclusion to change our general conclusions.

Two frequently invoked explanations for this anticorrelation of the strong bar fraction with H I gas mass ratio are that (i) bars promote the consumption of atomic gas and (ii) gas in disk galaxies inhibits the formation of bars and/or prevents their growth. Here, we want to explore if either of these two hypotheses are able to explain the decrease of the bar fraction with increasing H I gas mass fraction found in our sample.

If galaxies with strong bars consume their H I gas faster than unbarred ones, we expect that for a given $M_{\rm H\,I}/M_*$ ratio, galaxies with strong bars would be consuming their gas at a higher rate than unbarred galaxies, presenting a higher star formation activity. In Figure 6 (top panel) we plot the Hα equivalent width as a function of $M_{\rm H\,I}/M_*$ for galaxies hosting strong bars, weak bars, and unbarred galaxies. We use W(Hα) as an indicator of SFR in the central region of galaxies ($R < 1\farcs5$). Within error bars, we do not find any statistical difference for the value of W(Hα) at fixed $M_{\rm H\,I}/M_*$ between barred and unbarred galaxies.

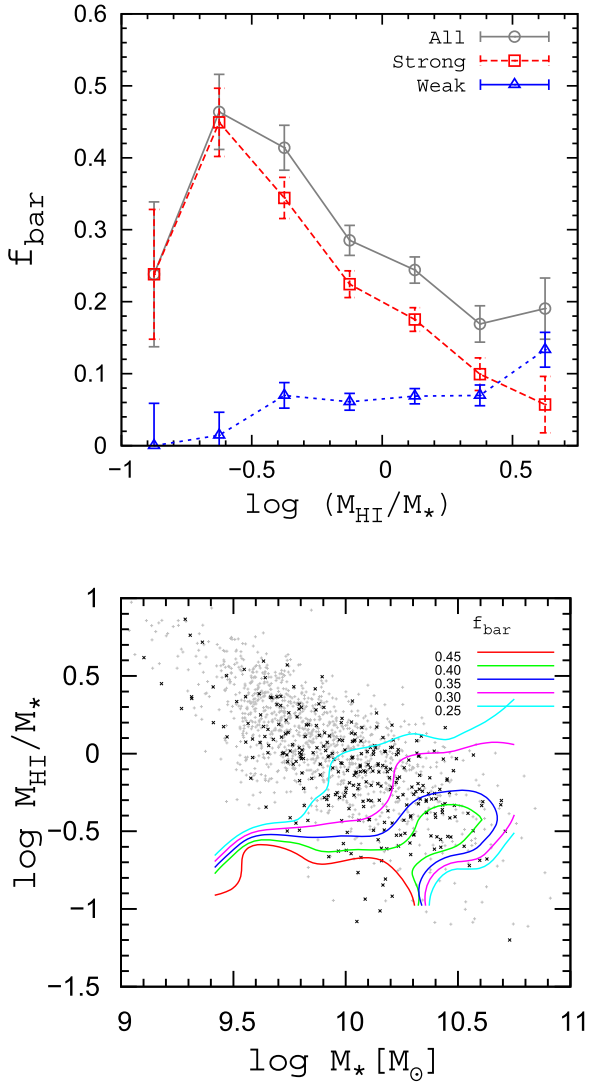

Figure 5. (Top panel) Bar fraction as a function of H I gas mass fraction for strong, weak, and strong plus weak bars in our sample. (Bottom panel) Strong bar fraction in the $M_{\rm H\,I}/M_*$ vs. M_* plane. Contours denote regions of constant $f_{\rm bar}$ in the range $0.25 \leqslant f_{\rm bar} \leqslant 0.45$. Gray dots represent unbarred galaxies, black dots represent barred ones.

Figure 6 (middle panel) shows the sSFR as a function of H I gas mass ratio for the three subsamples. We find that the global sSFR increases for increasing $M_{\rm H\,I}/M_*$, with unbarred galaxies having systematically higher sSFR than strongly barred galaxies for a given $M_{\rm H\,I}/M_*$ value, a trend in the opposite direction of the one expected if strong bars in galaxies promote gas consumption.

An alternative possibility to explore this hypothesis is looking at the bar fraction as a function of the gas consumption timescale, defined as $t_{\rm cons} = M_{\rm H\,I}/{\rm SFR}$ (Roberts 1963), which is the time a galaxy would take to consume its H I gas mass if its star formation continues at the same rate as at present. It is important to keep in mind that this is just a rough estimate of the time that galaxies can sustain a certain amount of star formation. Even in a closed box scenario, given the tight correlation between the SFR and the gas column density

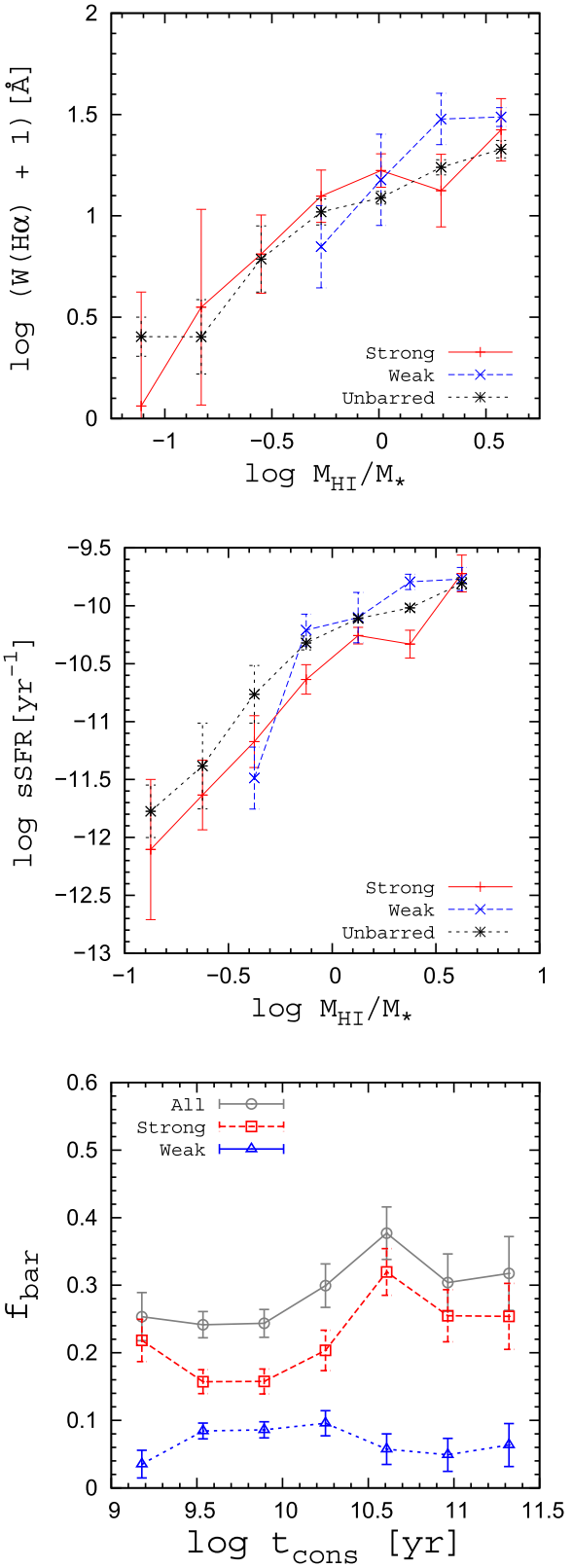

Figure 6. (Top panel) Dependence of the equivalent width of the Hα line on $M_{\rm H\,I}/M_*$ for galaxies with strong bars, weak bars, and unbarred galaxies. (Middle panel) Dependence of sSFR on $M_{\rm H\,I}/M_*$ for galaxies with strong bars, weak bars, and unbarred galaxies. (Bottom panel) Dependence of the bar fraction on $t_{\rm cons}$.

(Kennicutt 1998), a decrease in the gas column density due to star formation would decrease the star formation which in turn decreases t_{cons}. In a more realistic scenario, gas can be accreated into galaxies, but unless barred and unbarred galaxies are accreating gas at different rates, we still can compare gas consumption timescales for each sub-sample to draw general conclusions. If the trend between f_{bar} and $M_{H\,I}/M_*$ is caused by the quick consumption of atomic gas in barred galaxies, the bar fraction should be higher in galaxies with short gas consumption timescales. As we observe in Figure 6 (bottom panel) this is not the case. The bar fraction presents only a weak dependence on t_{cons}, with a mild increase of f_{bar} with increasing t_{cons} for strong bars, a trend in the opposite direction of the one expected according to our hypothesis.

This quenching of star formation in barred galaxies is not unheard-of, and has actually been recently reported by several authors (Wang et al. 2012; Cheung et al. 2013; Gavazzi et al. 2015), especially for the case of massive galaxies, where the bar might have funneled a large proportion of gas to the central region, causing a brief but strong burst of star formation, starving the outer regions, and turning the galaxy into a quiescent one.

The results presented in Figure 6 favor the explanation where the low bar fraction in H I gas-rich galaxies is not a result of strong bars promoting the quick consumption of gas, but is a result of the effect of gas on bar formation. The effect of the gas on bar formation and evolution has been addressed by several theoretical studies. Berentzen et al. (2007), studying the evolution of a live disk–halo system found that in gas-rich disks, the bar funnels gas to the central region where it forms a CMC that in turn weakens the bar. In the simulations by Villa-Vargas et al. (2010), bars are prevented to grow in gas-rich disks. Athanassoula et al. (2013) reported that in their *N*-body simulations, long-scale bars form later in gas-rich systems than in gas-poor ones, and that these bars are weaker in gas-rich cases. They attribute this to the formation of CMCs that are formed in gas-rich systems when gas is pushed inwards, also arguing that gas might transfer angular momentum to the bar, hindering its growth.

Finally, as stars are formed in thin disks of gas that gradually thicken through dynamical effects, gas-rich galaxies are expected to present more prominent thin disks than gas-poor galaxies. Klypin et al. (2009) reported slowly rotating long bars in their thick disk models, in contrast with the rapidly rotating shorter bars present in the thin disks, which following the previous argument favors the formation of strong, slowly rotating bars in gas-poor systems.

4. CONCLUSIONS

Using a sample of galaxies from the SDSS where bars are visually identified, and using H I mass and kinematic information from ALFALFA, we studied the fraction of galaxies hosting bars as a function of stellar and baryonic masses, as well as two estimates of halo mass. We found an increase of f_{bar} for strong bars, with increasing stellar and baryonic masses, with a stronger dependence on M_* than on $M_{baryonic}$. The signal of the correlation of the bar fraction with halo mass estimates is weak.

We confirm previous results by CS+15 and Díaz-García et al. (2016), finding an increase of the strong bar fraction with increasing stellar-to-halo mass ratio. For massive galaxies in our sample, with $M_* > 10^{10}\ M_\odot$, the dependence of the bar fraction on M_{dyn} and M_{halo} is present even at fixed M_*, with decreasing f_{bar} for increasing global halo mass, measured to a distance of the order of the H I disk extent. Compared with the dependence of f_{bar} on stellar mass, the dependence of f_{bar} on the dynamical and halo masses is small.

We find a strong correlation between the bar fraction and the H I gas mass ratio, such that the strong bar fraction decreases with increasing atomic gas content, in good agreement with Masters et al. (2012). The dependence of f_{bar} with $M_{H\,I}/M_*$ is usually explained invoking two mechanisms: (i) strong bars promote the consumption of atomic gas and (ii) gas prevents the formation/growth of bars. Our results show that barred galaxies in our sample are not consuming their gas in a more efficient way than their unbarred counterparts, hence favoring the second explanation; increasing the gas content in disk galaxies prevents the formation of bars, they grow more slowly or they are destroyed directly or indirectly by the presence of gas, as explained by recent theoretical works (Berentzen et al. 2007; Villa-Vargas et al. 2010; Athanassoula et al. 2013; Algorry et al. 2016).

The author thanks Changbom Park for providing the sample for the present study, and S. Courteau and IRyA Extragalactic group for valuable discussions about the results. The author acknowledges financial support through PAPIIT project IA103517 from DGAPA-UNAM. The author also thanks the anonymous referee for useful comments that helped to improve the quality of the paper and clarify the results. Funding for the SDSS and SDSS-II has been provided by the Alfred P. Sloan Foundation, the Participating Institutions, the National Science Foundation, the U.S. Department of Energy, the National Aeronautics and Space Administration, the Japanese Monbukagakusho, the Max Planck Society, and the Higher Education Funding Council for England. The SDSS Web Site is http://www.sdss.org/. The SDSS is managed by the Astrophysical Research Consortium for the Participating Institutions. The Participating Institutions are the American Museum of Natural History, Astrophysical Institute Potsdam, University of Basel, University of Cambridge, Case Western Reserve University, University of Chicago, Drexel University, Fermilab, the Institute for Advanced Study, the Japan Participation Group, Johns Hopkins University, the Joint Institute for Nuclear Astrophysics, the Kavli Institute for Particle Astrophysics and Cosmology, the Korean Scientist Group, the Chinese Academy of Sciences (LAMOST), Los Alamos National Laboratory, the Max-Planck-Institute for Astronomy (MPIA), the Max-Planck-Institute for Astrophysics (MPA), New Mexico State University, Ohio State University, University of Pittsburgh, University of Portsmouth, Princeton University, the United States Naval Observatory, and the University of Washington.

REFERENCES

Abazajian, K. N., Adelman-McCarthy, J. K., Agüeros, M. A., et al. 2009, ApJS, 182, 543
Algorry, D. G., Navarro, J. F., Abadi, M. G., et al. 2016, arXiv:1609.05909
Athanassoula, E. 1992, MNRAS, 259, 345
Athanassoula, E. 2002, ApJL, 569, L83
Athanassoula, E. 2003, MNRAS, 341, 1179
Athanassoula, E. 2013, Secular Evolution of Galaxies, 305
Athanassoula, E., Machado, R. E. G., & Rodionov, S. A. 2013, MNRAS, 429, 1949
Athanassoula, E., & Misiriotis, A. 2002, MNRAS, 330, 35
Athanassoula, E., & Sellwood, J. A. 1986, MNRAS, 221, 213

Berentzen, I., Heller, C. H., Shlosman, I., & Fricke, K. J. 1998, MNRAS, 300, 49
Berentzen, I., Shlosman, I., & Jogee, S. 2006, ApJ, 637, 582
Berentzen, I., Shlosman, I., Martinez-Valpuesta, I., & Heller, C. H. 2007, ApJ, 666, 189
Blanton, M. R., Kazin, E., Muna, D., Weaver, B. A., & Price-Whelan, A. 2011, AJ, 142, 31
Blanton, M. R., & Roweis, S. 2007, AJ, 133, 734
Blanton, M. R., Schlegel, D. J., Strauss, M. A., et al. 2005, AJ, 129, 2562
Bradford, J. D., Geha, M. C., & Blanton, M. R. 2015, ApJ, 809, 146
Brinchmann, J., Charlot, S., White, S. D. M., et al. 2004, MNRAS, 351, 1151
Broeils, A. H., & Rhee, M.-H. 1997, A&A, 324, 877
Buta, R. J., Sheth, K., Athanassoula, E., et al. 2015, ApJS, 217, 32
Buta, R. J., Sheth, K., Regan, M., et al. 2010, ApJS, 190, 147
Cervantes Sodi, B., Li, C., & Park, C. 2015, ApJ, 807, 111 (CS+15)
Cervantes-Sodi, B., Li, C., Park, C., & Wang, L. 2013, ApJ, 775, 19
Chabrier, G. 2003, PASP, 115, 763
Cheung, E., Athanassoula, E., Masters, K. L., et al. 2013, ApJ, 779, 162
Choi, Y.-Y., Han, D.-H., & Kim, S. S. 2010, JKAS, 43, 191
Christodoulou, D. M., Shlosman, I., & Tohline, J. E. 1995, ApJ, 443, 551
Combes, F. 2008, Formation and Evolution of Galaxy Bulges, 245, 151
Courteau, S., Andersen, D. R., Bershady, M. A., MacArthur, L. A., & Rix, H.-W. 2003, ApJ, 594, 208
Courtois, H. M., Tully, R. B., Fisher, J. R., et al. 2009, AJ, 138, 1938
Courtois, H. M., Tully, R. B., Makarov, D. I., et al. 2011, MNRAS, 414, 2005
de Vaucouleurs, G., de Vaucouleurs, A., Corwin, H. G., Jr., et al. 1991, Third Reference Catalogue of Bright Galaxies, Vol. 1–3 (Berlin: Springer)
Debattista, V. P., & Sellwood, J. A. 2000, ApJ, 543, 704
DeBuhr, J., Ma, C.-P., & White, S. D. M. 2012, MNRAS, 426, 983
Díaz-García, S., Salo, H., Laurikainen, E., & Herrera-Endoqui, M. 2016, A&A, 587, A160
Efstathiou, G., Lake, G., & Negroponte, J. 1982, MNRAS, 199, 1069
Ellison, S. L., Nair, P., Patton, D. R., et al. 2011, MNRAS, 416, 2182
Erwin, P. 2005, MNRAS, 364, 283
Eskridge, P. B., Frogel, J. A., Pogge, R. W., et al. 2000, AJ, 119, 536
Friedli, D., & Benz, W. 1993, A&A, 268, 65
Gavazzi, G., Consolandi, G., Dotti, M., et al. 2015, A&A, 580, A116
Giovanelli, R., Haynes, M. P., Kent, B. R., et al. 2005, AJ, 130, 2598
Giovanelli, R., Haynes, M. P., Salzer, J. J., et al. 1994, AJ, 107, 2036
Haynes, M. P., & Giovanelli, R. 1984, AJ, 89, 758
Haynes, M. P., Giovanelli, R., Martin, A. M., et al. 2011, AJ, 142, 170
Heller, C. H., & Shlosman, I. 1994, ApJ, 424, 84
Hoyle, B., Masters, K. L., Nichol, R. C., et al. 2011, MNRAS, 415, 3627
Jimenez, R., Padoan, P., Matteucci, F., & Heavens, A. F. 1998, MNRAS, 299, 123
Jogee, S., Scoville, N., & Kenney, J. D. P. 2005, ApJ, 630, 837
Kauffmann, G., Heckman, T. M., White, S. D. M., et al. 2003, MNRAS, 341, 33
Kennicutt, R. C., Jr. 1998, ARA&A, 36, 189
Kim, J.-H., & Lee, J. 2013, MNRAS, 432, 1701
Klypin, A., Valenzuela, O., Colín, P., & Quinn, T. 2009, MNRAS, 398, 1027
Knapen, J. H., Beckman, J. E., Heller, C. H., Shlosman, I., & de Jong, R. S. 1995, ApJ, 454, 623
Kormendy, J., & Kennicutt, R. C., Jr. 2004, ARA&A, 42, 603
Kraljic, K., Bournaud, F., & Martig, M. 2012, ApJ, 757, 60
Laurikainen, E., Salo, H., Buta, R., & Vasylyev, S. 2004, MNRAS, 355, 1251
Lee, G.-H., Park, C., Lee, M. G., & Choi, Y.-Y. 2012a, ApJ, 745, 125 (Lee+12)
Lee, G.-H., Woo, J.-H., Lee, M. G., et al. 2012b, ApJ, 750, 141
Lelli, F., McGaugh, S. S., & Schombert, J. M. 2016, AJ, 152, 157
Lin, Y., Cervantes Sodi, B., Li, C., Wang, L., & Wang, E. 2014, ApJ, 796, 98
Long, S., Shlosman, I., & Heller, C. 2014, ApJL, 783, L18
Lynden-Bell, D. 1979, MNRAS, 187, 101
Machado, R. E. G., & Athanassoula, E. 2010, MNRAS, 406, 2386
Martínez, H. J., & Muriel, H. 2011, MNRAS, 418, L148
Masters, K. L., Nichol, R. C., Haynes, M. P., et al. 2012, MNRAS, 424, 2180
Masters, K. L., Nichol, R. C., Hoyle, B., et al. 2011, MNRAS, 411, 2026
Nair, P. B., & Abraham, R. G. 2010, ApJL, 714, L260
Oh, S., Oh, K., & Yi, S. K. 2012, ApJS, 198, 4
Ostriker, J. P., & Peebles, P. J. E. 1973, ApJ, 186, 467
Park, C., & Choi, Y.-Y. 2005, ApJL, 635, L29
Roberts, M. S. 1963, ARA&A, 1, 149
Roberts, W. W., Jr., Huntley, J. M., & van Albada, G. D. 1979, ApJ, 233, 67
Saha, K., & Naab, T. 2013, MNRAS, 434, 1287
Saintonge, A., Catinella, B., Cortese, L., et al. 2016, MNRAS, 462, 1749
Sellwood, J. A. 1981, A&A, 99, 362
Sellwood, J. A. 2014, RvMP, 86, 1
Sellwood, J. A. 2016, ApJ, 819, 92
Sellwood, J. A., & Wilkinson, A. 1993, RPPh, 56, 173
Sheth, K., Elmegreen, D. M., Elmegreen, B. G., et al. 2008, ApJ, 675, 1141
Sheth, K., Vogel, S. N., Regan, M. W., Thornley, M. D., & Teuben, P. J. 2005, ApJ, 632, 217
Shlosman, I., Frank, J., & Begelman, M. C. 1989, Natur, 338, 45
Skibba, R. A., Masters, K. L., Nichol, R. C., et al. 2012, MNRAS, 423, 1485
Toomre, A. 1981, Structure and Evolution of Normal Galaxies, 111
van den Bosch, F. C. 2002, MNRAS, 332, 456
Villa-Vargas, J., Shlosman, I., & Heller, C. 2010, ApJ, 719, 1470
Wang, J., Kauffmann, G., Overzier, R., et al. 2012, MNRAS, 423, 3486
Weinberg, M. D. 1985, MNRAS, 213, 451
Weinzirl, T., Jogee, S., Khochfar, S., Burkert, A., & Kormendy, J. 2009, ApJ, 696, 411
Wilman, D. J., & Erwin, P. 2012, ApJ, 746, 160
Yang, X., Mo, H. J., van den Bosch, F. C., et al. 2007, ApJ, 671, 153
Yurin, D., & Springel, V. 2015, MNRAS, 452, 2367